Journal of Materials Chemistry A

Accepted Manuscript

ROYAL SOCIETY OF CHEMISTRY

www.rsc.org/materialsA

ECTFE porous membranes with conveniently controlled microstructures for vacuum membrane distillation

Jian Pan[a], Changfa Xiao[*a], Qinglin Huang[a], Hailiang Liu[a] and John. Hu[b]

[a] *State Key Laboratory of Separation Membranes and Membrane Processes, Tianjin Polytechnic University, Tianjin 300387, P. R. China*

E-mail: xiaochangfa@163.com; Tel.: +86 022 83955299

[b] *Technical Marketing Engineer, Solvay Specialty Polymers*

Abstract:

Poly(ethylene chlorotrifluoroethylene) (ECTFE) microporous membrane was prepared via thermally induced phase separation (TIPS) process using mixed diluent of bis(2-ethylhexyl) adipate (DEHA) and diethyl phthalate (DEP). The formation mechanism of ECTFE membrane was proposed with the assistance of a pseudo-binary temperature-DEHA ratio phase diagram of the ECTFE-diluent mixture system. The morphologies of prepared membranes were observed by scanning electron microscope (SEM) and atomic force microscope (AFM). Membranes' corresponding distillation performances were characterized in terms of porosity, contact angle, mechanical strength, permeability and rejection rate. The results showed that the evolution of membrane microstructure ranged in honeycomb, bicontinuous and spherulitic with increase of DEHA ratio. It was found that the membranes prepared via L-L phase separation had excellent hydrophobicity, high permeate flux and salt rejection ratio, and excellent anti-fouling property, especially for the membrane with DEHA/DEP mass ratio of 25wt.%/75wt.%.

1. Introduction

As global demand for water increases, the application of membrane technology on water purification has attracted increasing attention, because of its multiple advantages, including superior water product quality, simple control of operation, low cost and easy maintenance [1]. One novel polymeric membrane material, poly(ethylene chlorotrifluoroethylene) (ECTFE), has gained more and more attention due to its excellent properties. ECTFE is a semi-crystalline, thermoplastic copolymer which composed of alternating ethylene and chlorotrifluoroethylene units. It has excellent mechanical properties in a wide range of temperatures, with a continuous service temperature greater than 150^{o}C [2-3]. It is resistant to a wide variety of corrosive chemicals and organic solvents, including strong acids, chlorine, caustic solutions, strong polar solvents, and strong oxidizing agents. Thus, ECTFE is a promising material with strong potential in membrane separation processes that under harsh conditions [2, 4].

ECTFE is insoluble in all known solvents at room temperature [5], the fabrication of ECTFE membranes is not feasible via conventional methods such as solution phase inversion method. However, since ECTFE is soluble in selected solvents at elevated temperatures, it is possible to fabricate membranes via the thermally induced phase separation (TIPS) process, which is a useful technique for the preparation of polymeric membrane and has been applied to many polymers, such as PP [6-8], PE [9-10], PAN [11-12] and PVDF [13-16].

A few studies have been reported on preparation of ECTFE microporous membrane via TIPS [4, 17-20]. During the TIPS membrane formation process, a homogeneous polymer-diluent solution at an elevated temperature is cast or extruded into a desired shape and then cooled at a low temperature to induce phase separation and polymer solidification. The diluent is extracted by

appropriate extractant which is usually evaporated to form a microporous structure. When thermal energy is removed from a homogeneous polymer-diluent mixture, the TIPS can occur via solid-liquid or liquid-liquid phase separation depending on the polymer-diluent interaction, the composition and the thermal driving force [21-22]. In previous studies, only monotonous structure of ECTFE membranes prepared by ECTFE/single diluent systems were obtained. Blending additives, such as glycerol triacetate (GTA), triethyl citrate (CTF), dibutylitaconate (DBI) and diethyl adipate (DEA), had been tested in order to improve polymer processability [4], it's main purpose was not to control the membrane structure. Although the different structure could be obtained by controlling the technological parameters, such as: casting solution composition, cooling rate, axial stretching [5], on the one hand the parameters were complicated to control, on the other hand the change of structure was not obvious. In order to obtain various structures of membranes prepared via TIPS process, several modified TIPS technologies were investigated, such as the thermally assisted evaporative phase separation [23] and the combined use of thermally induced phase separation and immersion precipitation [24]. Although novel membrane microstructures were created, these new processes had a large number of parameters to control the membrane structures.

Recently, preparation of membrane by using diluent mixture via TIPS process showed good results in controlling membrane structure. Ji et al. prepared PVDF microporous membranes using diluent mixture of dibutyl phthalate (DBP) and di(2-ethylhexyl) phthalate (DEHP), had been shown to easily produce membranes with various microstructures by only varying the DBP/DEHP ratio. [21] They found that the membrane prepared with diluent mixture of 30/70 (wt.%/wt.%) DBP/DEHP presented higher water permeability and high solute rejection property [22]. Shang et al. used a mixture of 1,3-propanediol and glycerol as the diluent to prepare EVOH membranes. When

the ratio of 1,3-propanediol to glycerol was 50:50, the membrane showed about 100 times higher water permeability than the membrane prepared with pure glycerol. [25] Moreover, regular and highly interconnected macroporous scaffolds were fabricated from PLGA-dioxane-water ternary systems without any surfactant or other additives [26], and the structure of membrane made of PE had been controlled systematically by using various diluent mixture, such as polytetramethylene glycol (PTMG) and paraffin [27], dioctyl phthalate (DOP) and isoparaffin [28], ditrydecylphthalate and hexadecane [29]. All the previous studies proved that, the using of diluent mixture was an efficient and handy method to control membrane structure via changing the interaction between polymer and diluent mixture with only varying the composition of diluent mixture.

In this study, ECTFE porous membranes were prepared along with diluent mixture (bis(2-ethylhexyl) adipate (DEHA)/diethyl phthalate (DEP)) via the TIPS process at temperatures below ECTFE's melting point. The objective of this study was to demonstrate the effect of the interaction between diluent and polymer on the structure of membrane, and to control the structure of membrane systematically by varying the composition of diluent mixture. The effects of membrane structure on the performance of membranes were also discussed.

2. Experimental section

2.1. Materials

The ECTFE used in this study was provided by Solvay Specialty Polymers (Halar® 902). DEHA and DEP supplied by Shandong Kexing Chemical Co., Ltd. and Tianjin Guangfu Fine Chemical Research Institute, respectively, were used for preparing diluent mixtures without further purification. Both DEHA (b.p. 417^{o}C) and DEP (b.p. 302^{o}C) had boiling points higher than the melting point of ECTFE (242^{o}C) [3] and they were miscible with each other. Molecular weight,

density and solubility parameter for ECTFE and diluents were listed in Table 1.

Table 1 Molecular weight, density and solubility parameter for ECTFE and diluents

Substance	Molecular weight	Density (g/cm^3)[a]	Solubility parameter ($MPa^{1/2}$)[a]
DEHA	370.57	0.928	17.8
DEP	222.24	1.118	20.5
ECTFE	-	1.68	17.3

[a] Ref. [30].

2.2. Phase diagram

Homogeneous diluent mixtures (DEHA/DEP) of known concentration were prepared beforehand. ECTFE and the diluents were mixed at an elevated temperature (250°C) for at least 3h in a glass vessel with a stirrer. Then the glass vessel was quenched in liquid nitrogen to solidify the sample, and broken open to obtain the solid polymer-diluent sample. Homogeneous solid samples of 20 wt.% ECTFE with diluent mixtures of various DEHA/DEP ratios were prepared.

Each solid sample was then chopped into small pieces and placed between a pair of microscope cover slips and a Teflon film with a circle opening in the center was inserted between the cover slips to prevent diluent loss by evaporation. The sample was heated on a hot stage (THMS 600, Linkam, UK) to 250°C at 10°C/min and held for 1min, then cooled to 40°C at a rate of 10°C/min. The cloud point (T_{cloud}) was determined visually by the appearance of turbidity under an optical microscope (5050zoom, Olympus Co., Japan). A DSC (DSC 200 F3, Netzsch, Germany) was used to determine the crystallization temperature (T_c). The solid sample was sealed in an aluminum differential scanning calorimetry pan, melted at 250°C for 5min to erase thermal history and cooled to 40°C at 10°C/min, the temperatures of the exothermic peak during the cooling were

taken as T_c.

2.3. Preparation of the porous membrane

Homogeneous polymer-diluent samples were placed on a stainless steel mould (Fig. 1). A layer of polyimide film was applied to the inner side of the upper cover slip to prevent diluent loss by evaporation. The samples were heated at 210°C (250°C for only DEP system) for 10min on the heater and were pressed to films. And then the mould containing the film was cooled to room temperature with cooling water. The diluent in the film was extracted by immersing in ethanol for 24h and in pure water for 24h. The final membranes were freeze-dried using a freeze dryer (FD-1D-80, Shanghai Hanuo Instruments Co., China). These membranes were named as M-d0, M-d10, M-d20, M-d25, M-d30, M-d40, M-d50 and M-d100 according to the diluent mixture used 0/100, 10/90, 20/80, 25/75, 30/70, 40/60, 50/50, 100/0 wt.%/wt.%. DEHA/DEP, respectively. The thickness of the membrane was adjusted by the mould to be 150 ± 5μm as shown in Fig. 1.

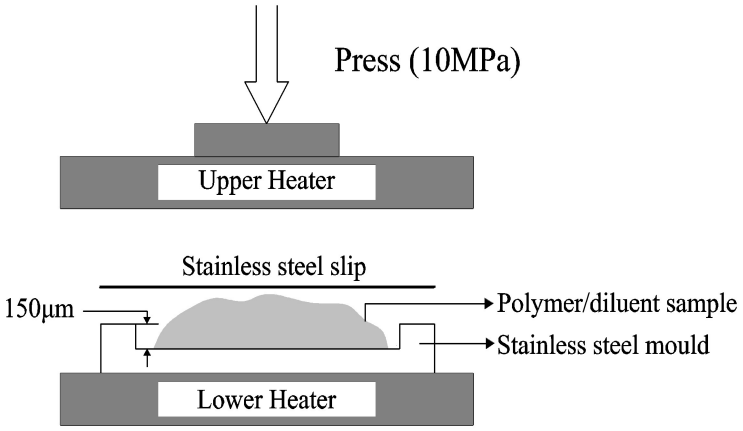

Fig. 1. Schematic diagram of hot-press apparatus for membrane preparation.

2.4. Characterization of the porous membrane

The dry membranes were freeze-fractured in liquid nitrogen and then sputter-coated with gold. The cross-sections and surfaces of the membranes were observed by a scanning electron

microscopy (SEM TM3030, Hitachi Co., Japan).

An atomic force microscope (AFM) (Multimode8, Bruker, Germany) was employed to analyze the surface states of the prepared membranes. All the membrane samples were measured by using a same tip and the surface roughness was obtained by tapping mode.

Membrane porosity was determined by gravimetric method following the procedure reported in literature [20,31]. Membranes were weighted dry and wet after the immersion in 1-Butanol for 24h. Porosity was calculated according to the following Eq. (1):

$$\varepsilon = \frac{(m_w - m_d)/\rho_w}{(m_w - m_d)/\rho_w + m_d/\rho_p} \times 100\% \quad (1)$$

where m_w and m_d was the weight of the wet and dry membrane, respectively, ρ_w was the 1-Butanol density (0.81g/cm^3) and ρ_p was the density of ECTFE (1.68g/cm^3) [3].

The average pore size of the membranes was evaluated by using Automatic Mercury Porosimeter (AutoPore IV-9500, Tektronix, USA).

Water contact angle of the membranes was measured using a contact angle goniometer (DSA-100, Kruss, Germany) at room temperature. A 3μL droplet of water was dropped on the surface of membrane and the water contact angle was measured automatically. Each sample was measured 10 times at different positions and the average value was calculated.

Mechanical strength of the membranes was conducted using a tensile testing instrument (YG061F, Laizhou Electron Instrument Co., China). The membrane samples were cut into 5mm (width) × 50mm (length) test strips, the tensile rate was 25mm/min. Every specimen was tested by 10 times.

The pure water flux (PWF) of pre-wetted membranes was determined by the following Eq. (2), the pressure across the membrane was 0.1MPa:

$$J = V / (A \times t) \qquad (2)$$

where J was the PWF (L/(m^2·h)), V was the total permeation (L), A was the membrane area (m^2) and t was the sampling time (h).

Nitrogen flux of dry membranes was determined by the following Eq. (3), and the permeate flow rate was measured at 0.01MPa:

$$J = L / A \qquad (3)$$

where J was the Nitrogen flux (m^3/(m^2·h)), L was the Nitrogen flow (m^3/h) and A was the membrane area (m^2).

Liquid entrance pressure (LEP) of dry membranes was measured using a laboratory device (Fig. 2) at room temperature. Increased the pressure slowly until the mutation of the conductivity meter, this mutation pressure was considered as the LEP point. Average of three tests was the LEP of the membrane.

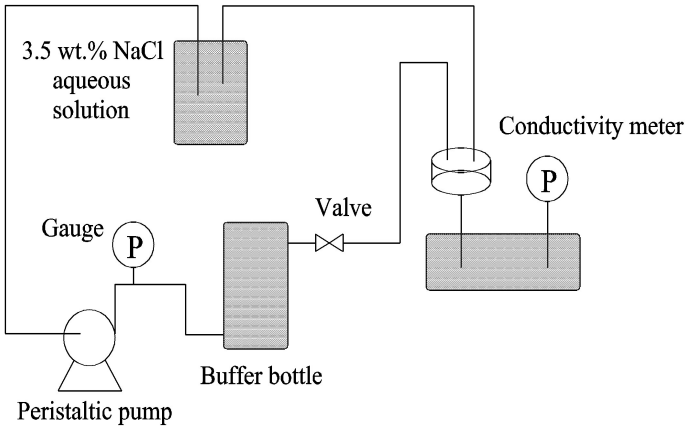

Fig. 2. LEP of the flat-sheet membrane testing device.

2.5. Distillation experiment

The schematic diagram of vacuum membrane distillation (VMD) devices was shown in Fig. 3. All of the system piping and storage tanks were thoroughly insulated to minimize heat loss to

the environment. 3.5wt.% NaCl solution was adopted as feed. In the feed circulating tank, the feed solution was heated to 80°C by a constant temperature heating device, and then pumped into the shell side of the membrane module at 2.75LPM. After being evaporated in the module, the feed flowed back to the circulating tank to be heated again. A vacuum pump was used to create a vacuum condition inside the tube side of the membrane module. The vacuum pressure was adjusted to 0.095MPa by the gas regulating valve. A heat exchanger was employed to condense the water vapor obtained from the membrane module. The condensate was collected and measured by conductivity meter (FE30K, Mettler Toledo, China) and liquid level gauge, the liquid level was read as the key data for calculating permeate flux (J_o).

The NaCl rejection ratio R was calculated by Eq. (4):

$$R = (1 - \frac{C_p}{C_f}) \times 100\% \qquad (4)$$

where C_f and C_p was the conductivity of the feed solution and permeate water, respectively.

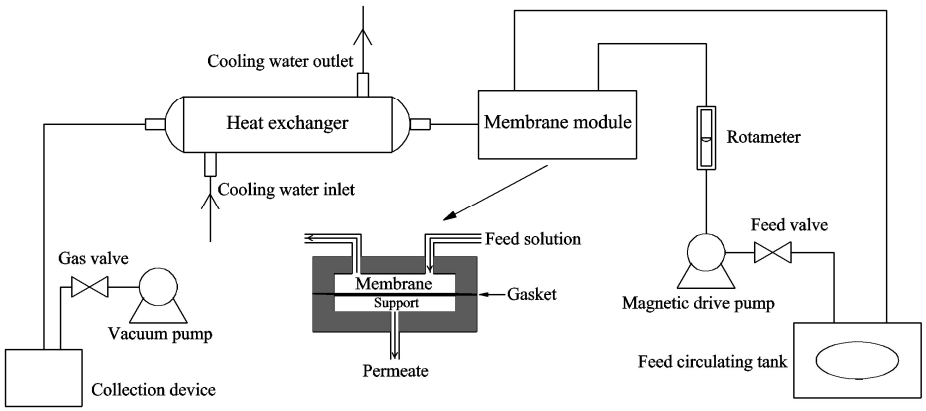

Fig. 3. Schematic diagram of the experimental VMD apparatus.

After each experiment, the membrane was repeatedly flushed with distilled water, dried in the air. Then the permeate flux (J_q) of the cleaned membrane was tested again by repeating the above

distillation experiment.

In order to evaluate the fouling-resistance of the membrane, the flux recovery ratio (FRR) was calculated by using the following Eq. (5):

$$FRR = \frac{J_q}{J_o} \times 100\% \qquad (5)$$

3. Results and discussion

3.1. Phase diagram

The phase diagram of 20wt.% ECTFE samples prepared with several diluent mixtures of different DEHA/DEP mass ratios was shown in Fig. 4. As seen in Fig. 4, T_{cloud} decreased significantly with the increased DEHA content, while T_c decreased slowly. When the DEHA/DEP mass ratio in diluent mixtures reached 32wt.%/68wt.%, L-L phase separation was no longer observed experimentally, and only the polymer crystallization process was present. Besides, with the addition of DEHA (Synonym, DOA), the temperature of the formation of a homogeneous ECTFE-diluents system reduced obviously as experimental results showed in section *2.3.* and also as our previous study [32].

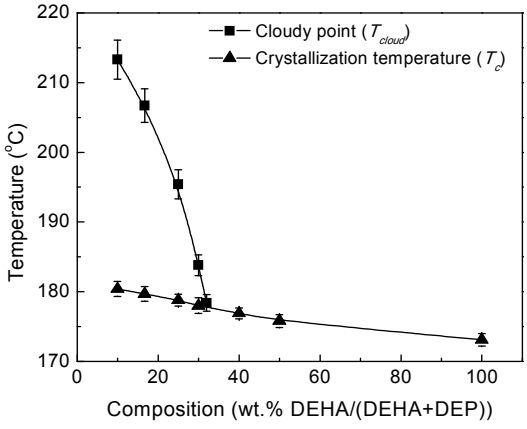

Fig. 4. Phase diagram of 20wt.% ECTFE samples prepared with several diluent mixtures of different DEHA

content.

The overall feature in Fig. 4 was analyzed in terms of the interaction between ECTFE and diluent mixture. The interaction parameter χ, typically used to interpret the interaction between polymer and diluent, was calculated from the difference of the solubility parameters between them using the following Eq. (6) [30]:

$$\chi = \frac{V_i}{RT}(\delta_i - \delta_j)^2 + 0.34 \qquad (6)$$

where V_i was the molar volume of the diluent, $V_i=M_i/\rho_i$; δ_i, δ_j referred to the solubility parameter of the diluent and the polymer, respectively.

Subsequently, the value of molar volume and solubility parameter for mixed diluent could be calculated by the following equations [30]:

$$V_i = V_1\Phi_1 + V_2\Phi_2 = \frac{M_1}{\rho_1}\Phi_1 + \frac{M_2}{\rho_2}\Phi_2 \qquad (7)$$

$$\delta_i = \delta_1\Phi_1 + \delta_2\Phi_2 \qquad (8)$$

where Φ_1, V_1, δ_1 was the volume fraction, molar volume and solubility parameter of one diluent, respectively, meanwhile, Φ_2, V_2, δ_2 was those of another diluent, respectively. By combining Eqs. (6), (7) and (8) with the values of parameters for ECTFE and diluents in Table 1, χ could be determined as a function of the DEHA/DEP ratio, smaller value of χ presented better interaction between ECTFE and the diluent [25,30]. Plotting χ against the DEHA/DEP ratio in diluent mixture gave a straight line, as shown in Fig. 5.

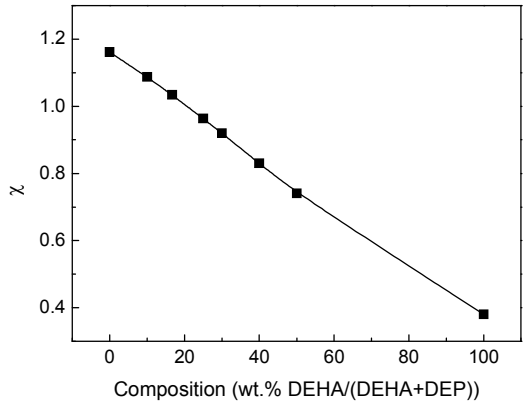

Fig. 5. Relation between DEHA content in diluent mixture and ECTFE-DEHA/DEP interaction parameter at 298K.

It was clear that χ was decreasing proportionally with the increase of DEHA/DEP ratio, which expressed that the increase of DEHA/DEP ratio enhanced the interaction between polymer and diluent mixture. As a result, the L-L phase separation happened before the crystallization owing to the poor interaction between polymer and diluent. As the interaction further enhanced, there was no more L-L phase separation appearing but only crystallization of polymer (S-L phase separation) [18,33].

On the other hand, stronger interaction between ECTFE and the diluent mixture led to lower mobility of polymer segments and thus prevented crystal nucleation and growth of ECTFE as DEHA content increased. As a result, the system needed deeper degree of super cooling to form the crystal nuclei of ECTFE and the crystallization temperature decreased as DEHA content increased. [21]

3.2. The microstructure of porous membranes

The evolution in the microstructure of membrane prepared via TIPS depended on the

thermodynamic and kinetic factors [34]. When the interaction between polymer and diluent was poor, the system would enter a metastable region at the early cooling stage and undergone the liquid-liquid phase separation. When the interaction between polymer and diluent was enhanced, the L-L phase separation shifted below the S-L phase, and only the crystal structure could be observed and controlled by varying cooling rate, polymer concentration and the interaction between polymer and diluent [35].

As described above, ECTFE could be dissolved in DEP or DEHA separately at an elevated temperature. Fig. 6 showed the SEM photographs of the cross-sections and surfaces of prepared porous membranes with a single diluent.

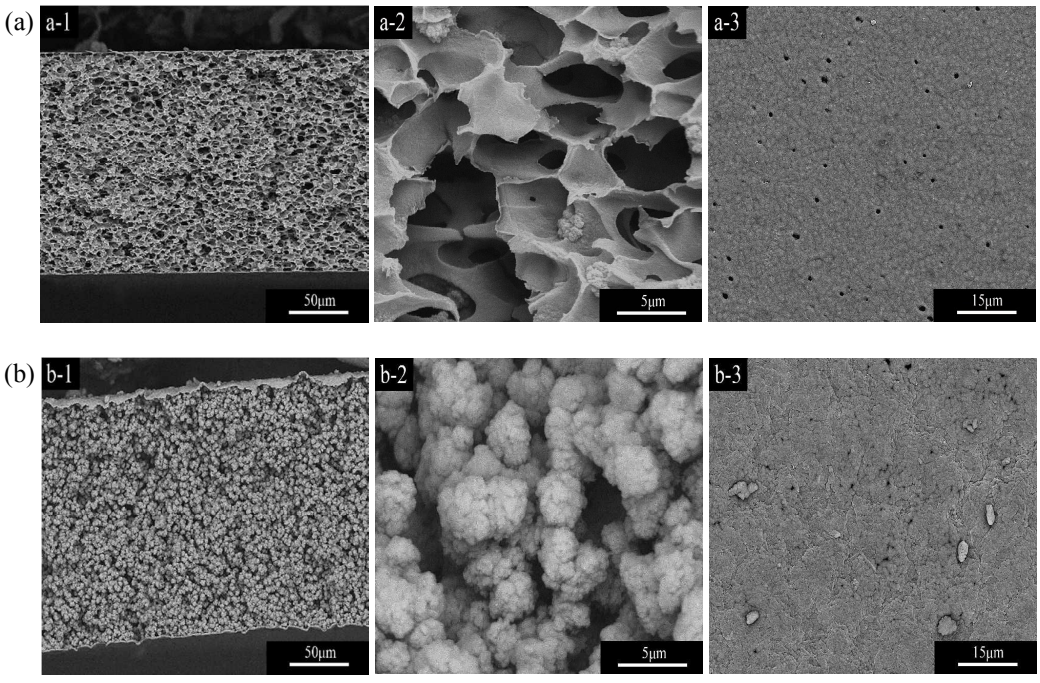

Fig. 6. SEM photographs of ECTFE porous membranes prepared with single diluent (a: M-d0, b: M-d100; 1: whole cross-section ×600, 2: enlarged cross-section ×7000, 3: the surface ×2000).

As the interaction between ECTFE and DEP was poor (shown in Fig. 5), the structure of

honeycomb pores, which was typical structure of membrane for system with L-L phase separation, was obtained in the cross-section of M-d0. To the contrary, the cross-sectional structure of M-d100 entirely presented spherulitic with S-L phase separation. [36,37] The surfaces of the two membranes both had a thin layer with low porosity.

For the conditions where the L-L phase separation was observed before crystallization, the effect of DEHA/DEP ratio on the cross-sectional and surface structures of membranes was shown in Fig. 7.

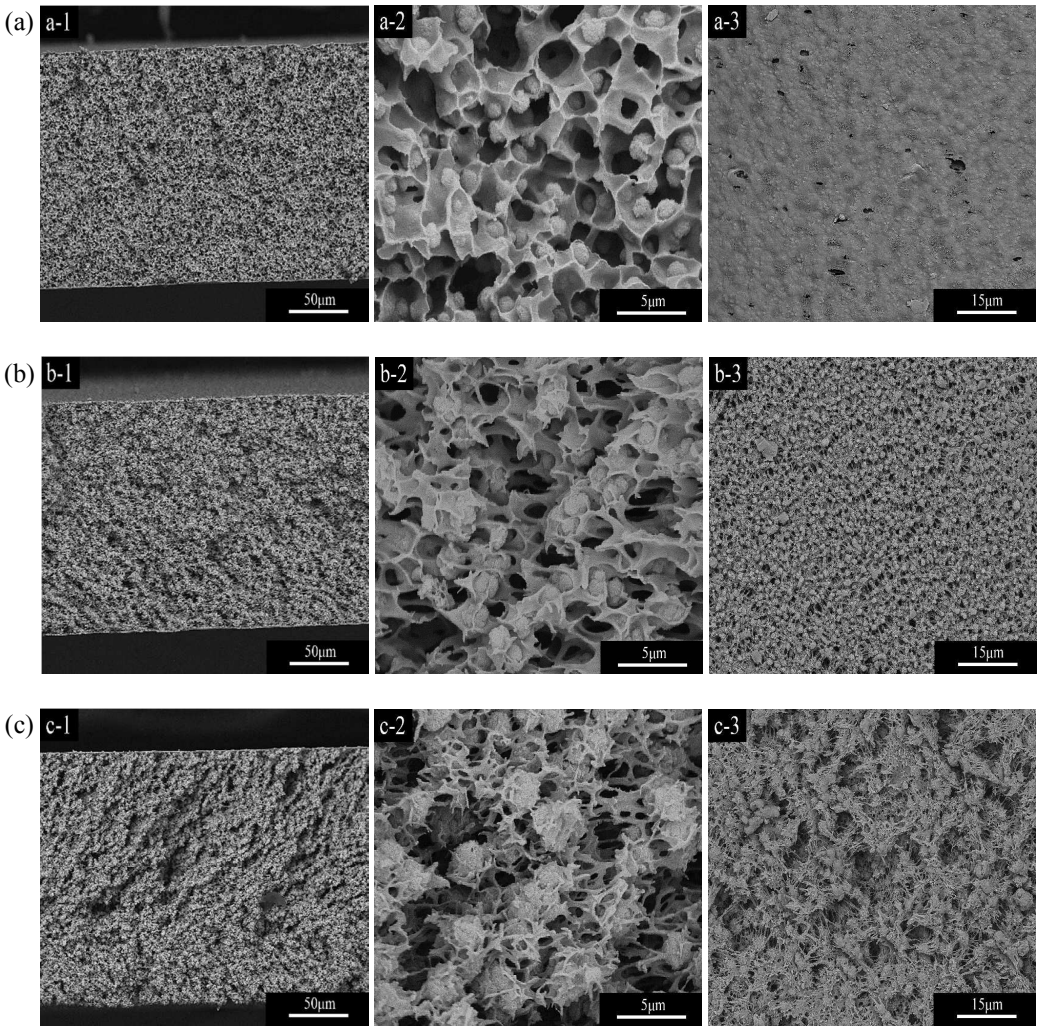

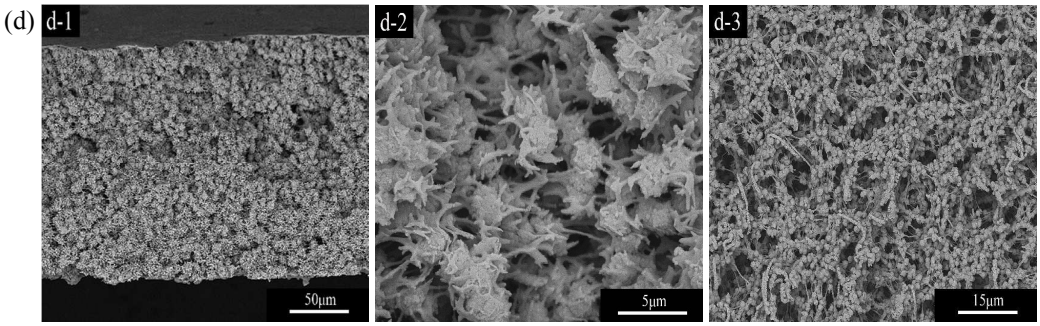

Fig. 7. SEM photographs of ECTFE porous membranes prepared via L-L phase separation with diluent mixture (a: M-d10, b: M-d20, c: M-d25, d: M-d30; 1: whole cross-section ×600, 2: enlarged cross-section ×7000, 3: the surface ×2000).

The temperature gap between L-L phase separation temperature and the crystallization temperature of polymer played an important role in determining the microstructure of the porous membrane. As shown in Fig. 4, the cloud points of the samples decreased rapidly with the increase of DEHA content, while the crystallization temperatures of them had almost no decline. When the cooling condition was the same, the samples with lower DEHA content had more time for L-L phase separation. As a result, the volume fraction of lean-polymer phase was larger, leading to the structure with larger pores. On the other hand, with the increase of DEHA content, the cloud points of samples were closer to their crystallization temperatures. The L-L phase separation did not have enough time to complete before the crystallization of ECTFE started to take place. The spherulitic structure was observed, and the samples with higher DEHA content had more time for the coarsening of spherulites.

Moreover, the surface topography and three-dimensional surface images of the membranes could be observed in Fig. 8. Roughness parameters were obtained with the AFM analysis software, the average roughness (R_a) for the image was defined as the arithmetic average of the absolute

values of the surface height deviations measured from the center plane.

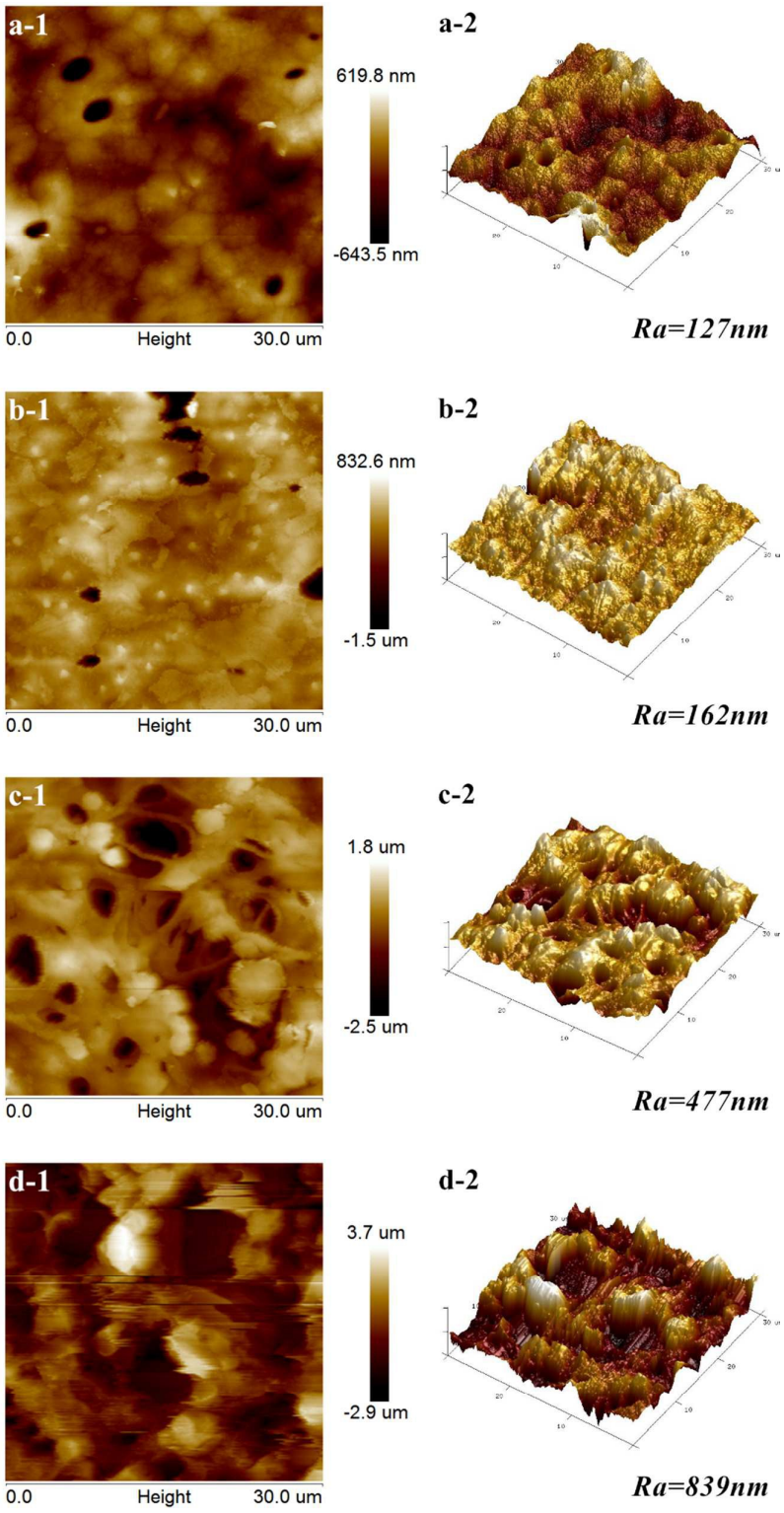

Fig. 8. AFM images of ECTFE porous membranes prepared via L-L phase separation with diluent mixture (a:

M-d10, b: M-d20, c: M-d25, d: M-d30; 1: surface topography, 2: three-dimensional surface).

Obviously, the surface porosity and roughness of the samples increased with the increase of DEHA content in the diluent mixture. The blurring in Fig. 8(d1) and the lack of details in Fig. 8(d2) were because of the roughness of M-d25 was so large that influenced the results of AFM testing.

The effect of DEHA/DEP ratio on the cross-sectional and surface structures of membranes where only crystallization was observed was shown in Fig. 9.

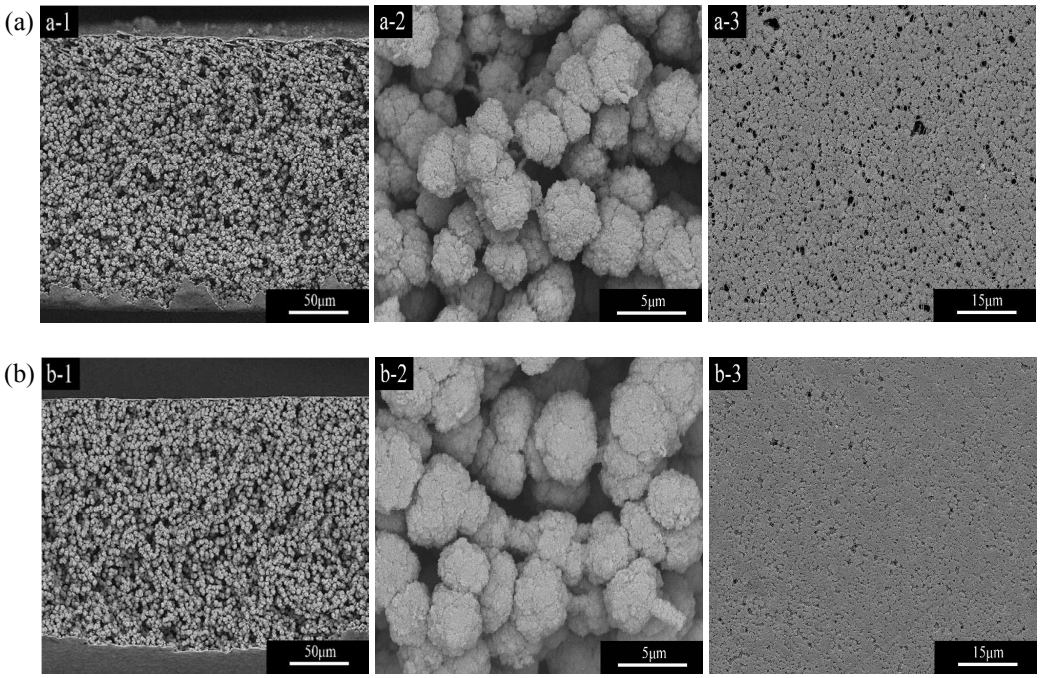

Fig. 9. SEM photographs of ECTFE porous membranes prepared via S-L phase separation with diluent mixture (a: M-d40, b: M-d50; 1: whole cross-section ×600, 2: enlarged cross-section ×7000, 3: the surface ×2000).

It could be seen that, the cross-sectional of M-d40 and M-d50 entirely presented spherulitic structure. The spherulites grew bigger and more perfectly progressively as the DEHA/DEP ratio

increased as shown in Fig. 9 and Fig. 6(b2). The system with higher DEHA/DEP ratio presented stronger interaction between ECTFE and diluent, which prevented the nucleation activity of ECTFE and led to the formation of few primary nuclei at the beginning of crystallization. Less primary nuclei had more polymer molecules to grow up, led to bigger pores, namely the space between spherulites. At the same time, the surface porosity of the samples decreased as the DEHA/DEP ratio increased, up to forming a thin layer as shown in Fig. 6(b3).

3.3. The mechanical properties of porous membranes

Mechanical properties measurements were undertaken on dry ECTFE porous membranes. Fig. 10 described the initial modulus, breaking strength and elongation of the membranes prepared by different diluent mixtures.

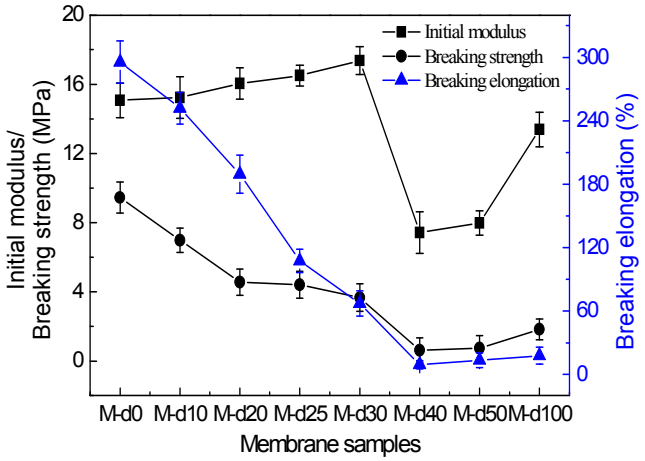

Fig. 10. Mechanical properties of the ECTFE porous membranes prepared by different diluent mixtures.

It was well known that the crystallinity and microstructure of membranes played two important roles on the mechanical properties of membranes. As shown in Fig. 10, the initial modulus increased slightly with the increase of DEHA content before the monotectic point, due to

the formation of closer spherulitic structure, but at the same time, both the strength- and elongation-at-break decreased gradually, that was mainly because the porous surface replaced the skin layer of the membranes as shown in Fig. 7(3). And then, with the continued increase of DEHA content, the bigger and bigger space between spherulites led to a rapid decrease of their mechanical properties.

3.4. Permeability of porous membranes

Some of typical properties and water, nitrogen gas permeability for the prepared ECTFE membranes were listed in Table 2 and Table 3. In Table 2, the increase of N_2 flux benefited from the increase of porosity, which was because the growing of spherulites among the honeycomb micropores formed more interconnected interfacial microvoids (IFMs) [38] as the increase of DEHA content. The rapid increase of surface roughness brought about the increase of water contact angle, indicated that the hydrophobicity of the prepared membranes increased. And the water could not permeate through the membranes with the operating pressure (0.1MPa), which was far below the LEP.

Table 2 Typical properties and permeability for M-d0, M-d10, M-d20, M-d25 and M-d30

Samples	Porosity (%)	Average pore size (μm)	SCA (^{o})	LEP (MPa)	N_2 flux ($m^3/(m^2 \cdot h)$)	PWF ($L/(m^2 \cdot h)$)
M-d0	65.1±6.1	0.26±0.02	93.4±7.8	0.27±0.03	10.4±1.8	-
M-d10	69.8±4.8	0.32±0.03	108.5±6.2	0.31±0.04	19.4±1.6	-
M-d20	73.3±4.4	0.37±0.02	119.3±7.4	0.38±0.02	22.9±2.0	-
M-d25	75.8±3.9	0.41±0.01	143.9±4.8	0.42±0.02	27.2±3.1	-
M-d30	74.9±5.0	0.38±0.02	141.2±5.3	0.29±0.03	26.6±2.4	-

Table 3 Typical properties and permeability for M-d40, M-d50 and M-d100

Samples	Porosity (%)	Average pore size (μm)	SCA (°)	LEP (MPa)	N_2 flux ($m^3/(m^2 \cdot h)$)	PWF ($L/(m^2 \cdot h)$)
M-d40	76.4±5.5	0.40±0.03	90.7±5.7	0.11±0.01	31.5±3.7	124.4±14.1
M-d50	78.5±6.2	0.38±0.02	83.3±6.0	0.10±0.02	34.7±2.9	144.9±12.7
M-d100	77.4±5.3	0.32±0.02	79.5±8.6	0.12±0.03	32.1±3.3	136.3±16.2

In Table 3, the structures of the three membranes were all prepared via only S-L phase separation. With the increase of DEHA content, the bigger space between spherulites led to the increase of porosity and N_2 flux. The loose spherulitic structure not only led to the low mechanical properties but also resulted in the low LEP, the decrease of water contact angle and LEP compared with the membranes obtained via L-L phase separation, indicated that the hydrophobicity of these membranes decreased. As the result, these membranes could not be applied to VMD with the water could permeate through them easily.

3.5. Membrane distillation performance

Membrane distillation (MD) was a membrane-based water treatment process where the driving force was a vapor pressure difference across the hydrophobic membrane. MD technology could be divided into four types according to its different condensation modes: direct contact membrane distillation (DCMD), air gap membrane distillation (AGMD), sweep gas membrane distillation (SGMD) and vacuum membrane distillation (VMD). Because of the low heat conduction loss and mass transfer resistance of the boundary layer, the permeate flux of VMD was higher than the other types [39]. In this study, M-d0, M-d10, M-d20, M-d25 and M-d30 were tested for VMD with feeding 3.5wt.% NaCl solution. The distillation results were shown in Fig. 11.

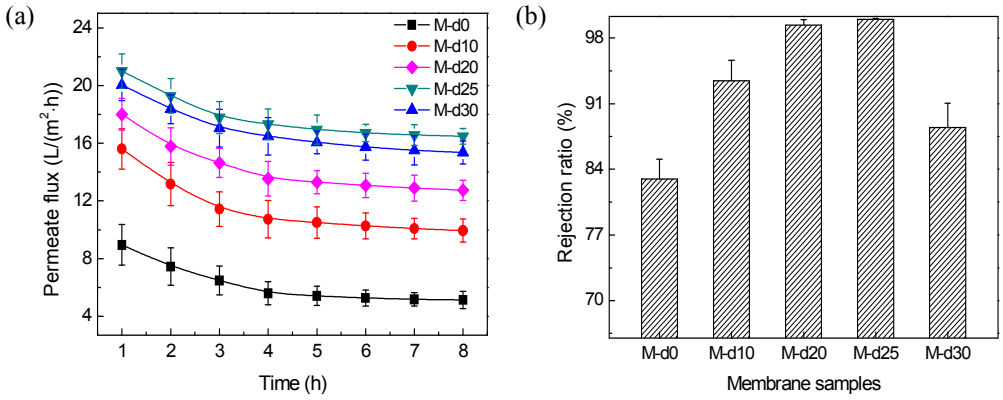

Fig. 11. Permeate flux as a function of running time (a) and NaCl rejection ratio (b) of the prepared membranes.

In Fig. 11(a), all the membranes could continuous running for 8 hours and even more, indicated the prepared membranes had good durability. The variation tendency of permeate flux was almost same as the variation of N_2 flux for the membrane samples. The increase of N_2 and permeate fluxes could be attributed to the increase of porosity, which not only reduced the thermosteresis of the heat transfer across the membrane, but also increased the mass transfer rate [40].

As two representations for the surface hydrophobicity of membrane, liquid entry pressure (or wetting pressure) and contact angle were the two important factors to determine the separation properties of the membranes in MD. The NaCl rejection results were shown in Fig. 11(b). There was an obvious growth trend of the rejection ratio as DEHA content increasing, it was because that the increase of contact angle was positive to promote the surface hydrophobicity of the membranes. Especially, the contact angle of M-d25 reached 143.9°, it's excellent hydrophobicity contributed to the highest separation accuracy, the rejection rate achieved 99.99%, and the conductivity of condensate was less than 5μs/cm. Besides, the contact angle of M-d30 was 141.2° higher than that of M-d20, but the rejection ratio was lower than latter, that was because it had

been influenced by a lower LEP. Under the pressure of feed solution's flowing and the negative pressure on the other side of the membrane, the compositive pressure applied on the membrane exceeded the LEP, then the salt solution penetrated the hydrophobic membrane. [40]

Furthermore, the MD performances of obtained membranes (M-d25) were compared with the commercial polymer membranes as summarized in Table 4 [41-44]. It was found that the permeate flux and salt rejection of the ECTFE membrane were both higher than the other membranes.

Table 4 Comparison of the flux obtained in this study with the literature for MD processes with flat-sheet membranes.

Reference	Application	Permeation flux ($L/(m^2 \cdot h)$)	NaCl rejection (%)	Feed solution	Feed inlet temperature (^oC)
[42]	DCMD	5.7	99.9	3.5 wt.% NaCl solution	80
[43]	VMD	11.8	97.0	3.5 wt.% NaCl solution	80
[44]	VMD	12.5	99.7	3.5 wt.% NaCl solution	80
M-d25	VMD	16.7	99.9	3.5 wt.% NaCl solution	80

In the long running process, the effects of membrane fouling, concentration polarization and temperature polarization were usually observed by a considerable decline in the flux with time. Thus the flux recovery ratio (FRR) was introduced to evaluate the fouling resistance properties. The recovery flux after water washing and FRR values for the membranes were presented in Fig. 12. It was observed that the change of permeate flux with time was same as Fig. 11(a), the decrease of flux with time was mainly because the concentration polarization and temperature polarization, rather than fouling under constant pressure. From Fig. 12(b), we could see that all FRR values were higher than 95%, and the maximum FRR value reached 98.8%, meaning the prepared membranes had excellent anti-fouling property, indicated the long-run utilization and operation reliability.

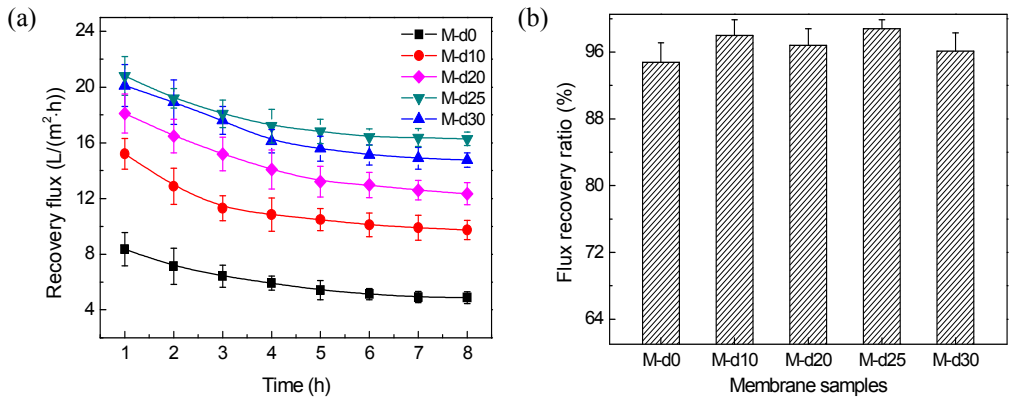

Fig. 12. Recovery flux as a function of running time (a) and flux recovery ratio (FRR) (b) of the prepared membranes.

4. Conclusion

ECTFE porous membranes were fabricated from a ternary system of ECTFE/DEHA/DEP for the first time via TIPS. The ratio of DEHA/DEP in diluent mixture obviously influenced on the structure and performance of the membranes. The results showed that, the low mechanical properties and poor hydrophobicity led the membranes prepared via S-L phase separation could not be used in membrane distillation. Via L-L phase separation, with the increase of DEHA content the structure of membranes ranged in honeycomb, bicontinuous and spherulitic; the porosity, surface roughness, hydrophobicity and permeate flux increased. Moreover, the membranes showed excellent fouling-resistance during continuous operation process of VMD. It was noteworthy that the stable permeate flux of the membrane with DEHA/DEP ratio of 25wt.%/75wt.% reached 16.5L/(m^2·h), combined with the salt rejection exceeded 99.99%.

Acknowledgements

The authors gratefully acknowledge the financial support of the National Basic Research

Program of China (2012CB722706) and the National Natural Science Foundation of China (21404079).

Notes and references

1. S. Rajabzadeh, C. Liang, Y. Ohmukai, T. Maruyama and H. Matsuyama, *J. Membr. Sci.*, 2012, **423-424**, 189-194.
2. Z. Cui, E. Drioli and Y. M. Lee, *Prog. Polym. Sci.*, 2014, **39**, 164-198.
3. Anonymous, *Halar® ECTFE design and processing guide*, http://www.solvayplastics.com, accessed Nov 2014.
4. S. Simone, A. Figoli, S. Santoro, F. Galiano, S. M. Alfadul, O. A. Al-Harbi and E. Drioli, *Sep. Purif. Technol.*, 2012, **90**, 147-161.
5. I. J. Roh, S. Ramaswamy, W. B. Krantz and A. R. Greenberg, *J. Membr. Sci.*, 2010, **362**, 211-220.
6. H. Matsuyama, T. Maki, M. Teramoto and K. Asano, *J. Membr. Sci.*, 2002, **204**, 323-328.
7. B. Luo, Z. Li, J. Zhang and X. Wang, *Desalination*, 2008, **233**, 19-31.
8. W. Yave, R. Quijada, M. Ulbricht and R. Benavente, *Polymer*, 2005, **46**, 11582-11590.
9. H. Matsuyama, H. Okafuji, T. Maki, M. Teramoto and N. Kubota, *J. Membr. Sci.*, 2003, **223**, 119-126.
10. M. J. Park and C. K. Kim, *J. Membr. Sci.*, 2014, **449**, 127-135.
11. Q.-Y. Wu, L.-S. Wan and Z.-K. Xu, *J. Membr. Sci.*, 2012, **409–410**, 355-364.
12. Q.-Y. Wu, L.-S. Wan and Z.-K. Xu, *RSC Adv.*, 2013, **3**, 17105-17112.
13. S. Rajabzadeh, T. Maruyama, T. Sotani and H. Matsuyama, *Sep. Purif. Technol.*, 2008, **63**, 415-423.
14. H.-Q. Liang, Q.-Y. Wu, L.-S. Wan, X.-J. Huang and Z.-K. Xu, *J. Membr. Sci.*, 2014, **465**, 56-67.
15. Z. Cui, N. T. Hassankiadeh, S. Y. Lee, J. M. Lee, K. T. Woo, A. Sanguineti, V. Arcella, Y. M. Lee and E. Drioli, *J. Membr. Sci.*, 2013, **444**, 223-236.
16. X. Li, G. Xu, X. Lu and C. Xiao, *J. Appl. Polym. Sci.*, 2008, **107**, 3630-3637.
17. S. Ramaswamy, A. R. Greenberg and W. B. Krantz, *J. Membr. Sci.*, 2002, **210**, 175-180.
18. B. Zhou, Y. Lin, W. Ma, Y. Tang, Y. Tian and X. Wang, *Chem. J. Chinese U.*, 2012, **33**, 2585-2590.
19. H.-J. Müller, *Desalination*, 2006, **199**, 191-192.
20. E. Drioli, S. Santoro, S. Simone, G. Barbieri, A. Brunetti, F. Macedonio and A. Figoli, *React. Funct. Polym.*, 2014, **79**, 1-7.
21. G.-L. Ji, B.-K. Zhu, Z.-Y. Cui, C.-F. Zhang and Y.-Y. Xu, *Polymer*, 2007, **48**, 6415-6425.
22. G. Ji, L. Zhu, B. Zhu, C. Zhang and Y. Xu, *J. Membr. Sci.*, 2008, **319**, 264-270.
23. D. Hellman, *J. Membr. Sci.*, 2004, **230**, 99-109.
24. H. Matsuyama, Y. Takida, T. Maki and M. Teramoto, *Polymer*, 2002, **43**, 5243-5248.
25. M. X. Shang, H. Matsuyama, M. Teramoto, J. Okuno, D. R. Lloyd and N. Kubota, *J. Appl. Polym. Sci.*, 2005, **95**, 219-225.

26. F. J. Hua, T. G. Park and D. S. Lee, *Polymer*, 2003, **44**, 1911-1920.
27. S. C. Roh, M. J. Park, S. H. Yoo and C. K. Kim, *J. Membr. Sci.*, 2012, **411–412**, 201-210.
28. L. U. Kim and C. K. Kim, *J. Polym. Sci., Part B: Polym. Phys.*, 2006, **44**, 2025-2034.
29. H. C. Vadalia, H. K. Lee, A. S. Myerson and K. Levon, *J. Membr. Sci.*, 1994, **89**, 37-50.
30. J. Brandrup, E. H. Immergut and E. A. Grulke, *Polymer Handbook (fourth edition)*, John Wiley & Sons, New York, 1999.
31. Z. Song, M. Xing, J. Zhang, B. Li and S. Wang, *Sep. Purif. Technol.*, 2012, **90**, 221-230.
32. J. Pan, C. Xiao, Q. Huang, C. Wang and H. Liu, *RSC Adv.*, 2015, **5**, 45249-45257.
33. D. R. Lloyd, S. S. Kim and K. E. Kinzer, *J. Membr. Sci.*, 1991, **64**, 1-11.
34. P. van de Witte, P. J. Dijkstra, J. W. A. van den Berg and J. Feijen, *J. Membr. Sci.*, 1996, **117**, 1-31.
35. H. Matsuyama, T. Iwatani, Y. Kitamura, M. Tearamoto and N. Sugoh, *J. Appl. Polym. Sci.*, 2001, **79**, 2449-2455.
36. H. Matsuyama, M. Teramoto, S. Kundari and Y. Kitamura, *J. Appl. Polym. Sci.*, 2001, **82**, 169-177.
37. M. Gu, J. Zhang, X. Wang, H. Tao and L. Ge, *Desalination*, 2006, **192**, 160-167.
38. Q. Huang, C. Xiao, X. Hu and S. An, *J. Mater. Chem.*, 2011, **21**, 16510.
39. L. Sun, L. Wang, Z. Wang, B. Li and S. Wang, *J. Membr. Sci.*, 2015, **488**, 30-39.
40. A. Alkhudhiri, N. Darwish and N. Hilal, *Desalination*, 2012, **287**, 2-18.
41. Y. Wu, Q. Huang, C. Xiao, K. Chen, X. Li and N. Li, *Desalination*, 2014, **353**, 118-124.
42. J. A. Prince, G. Singh, D. Rana, T. Matsuura, V. Anbharasi and T. S. Shanmugasundaram, *J. Membr. Sci.*, 2012, **397-398**, 80-86.
43. C. -K. Chiam and R. Sarbatly, *Chem. Eng. Process.*, 2014, **79**, 23-33.
44. H. Fan and Y. Peng, *Chem. Eng. Sci.*, 2012, **79**, 94-102.